Tellus (2004), 56A, 68–78
Printed in UK. All rights reserved

TELLUS

On the spontaneous transition to asymmetric thermohaline circulation

By JOHAN NILSSON[1]*, GÖRAN BROSTRÖM[1] and GÖSTA WALIN[2], [1]*Department of Meteorology, Stockholm University, SE-10691 Stockholm, Sweden;* [2]*Department of Oceanography, Earth Sciences Centre, Göteborg University, Box 460, SE-40530 Göteborg, Sweden*

(Manuscript received 19 May 2003; in final form 19 September 2003)

ABSTRACT

The stability of symmetric thermally dominated thermohaline circulation in a two-hemisphere basin is explored with the aid of a conceptual as well as a numerical model. The conceptual model has two layers, representing the water masses of the thermocline and the deep ocean, respectively. The stability of the symmetric solutions of the model to small symmetric or antisymmetric perturbations are considered. It is found that the symmetric equilibria are considerably more sensitive to antisymmetric than to symmetric perturbations. The reason is that a symmetric flow anomaly by necessity causes a perturbation of the thermocline depth; a state of affairs which provides a negative feedback. The strength of this stabilizing feedback depends on the properties of the vertical mixing in the interior ocean. In contrast, the antisymmetric flow perturbations assume a pole-to-pole overturning pattern with negligible vertical motion at low latitudes; this essentially removes the stabilizing feedback due to thermocline–depth adjustment. As a consequence, the dynamics of antisymmetric perturbations are basically independent of the vertical mixing. It is concluded that the symmetric circulation is always unstable to antisymmetric perturbations if $\Delta\rho_S/\Delta\rho_T > \frac{1}{2}$, where $\Delta\rho_S$ and $\Delta\rho_T$ are the equator-to-pole density contrasts created by salinity and temperature, respectively. However, if the interhemispheric density gradients in the deep ocean are assumed to strengthen the antisymmetric flow anomaly, the instability should occur for a considerably smaller value of $\Delta\rho_S/\Delta\rho_T$. Numerical simulations are presented that support the theoretical results and furthermore suggest that the density gradients in the deep ocean indeed augment the antisymmetric flow perturbations, thereby acting to destabilize the symmetric branch of thermally dominated circulation.

1. Introduction

In the present-day Atlantic and Pacific Oceans, the hydrographic fields are notably asymmetric with respect to the equator. This tendency is more pronounced in the salinity field than in the temperature field, although the two fields tend to be correlated. The salinity field in the Atlantic Ocean provides a striking illustration, where it appears as the tropical pool of warm saline water has tipped into the Northern Hemisphere (see e.g. Pickard and Emery 1982). There are two conceivable mechanisms behind the equatorial asymmetry in the World Ocean. *Pro primo*, it may be a consequence of asymmetries in the forcing fields and in the geometry of the ocean basins (e.g. Dijkstra and Neelin 2000). *Pro secundo*, a nearly symmetric state may exist in principle but is unstable. According to this view, the present skewed state is the result of a spontaneous symmetry breaking. Even if the forcing and the geometry were perfectly symmetric, the ocean would attain an asymmetric state.

*Corresponding author.
e-mail: nilsson@misu.su.se

Walin (1985) advanced the idea that a symmetric thermohaline circulation is unstable to antisymmetric perturbations when the freshwater forcing exceeds a threshold value. Based on considerations of a conceptual model, Walin suggested that a transition to asymmetric circulation occurs when the salinity field has removed half of the equator-to-pole density contrast associated with the thermal field. Furthermore, Walin underlined that the hydrographic skewness in the World Ocean could be shaped by spontaneous symmetry breaking. In fact, Rooth (1982) had a few years earlier advanced similar ideas and presented another conceptual model. A difference, however, is that Rooth's model does not allow for symmetric circulation, rather it yields a pole-to-pole circulation even for infinitely weak freshwater forcing (e.g. Welander, 1986; Scott et al., 1999). The notion that a symmetric thermohaline circulation, if perturbed, can make a transition to an asymmetric state gained a wider recognition through the pioneering numerical simulations by Bryan (1986) and Marotzke et al. (1988).

The present study deals with the stability of symmetric thermohaline circulation in the forward thermally dominated regime, where cold deep water is formed at high latitudes. Specifically,

we consider flows in a two-hemisphere basin forced by boundary conditions that are equatorially symmetric and time independent.[1] The penetrating study of Weijer and Dijkstra (2001) illuminates some key features concerning the stability of the thermohaline circulation in this geometry. In particular, their analyses show that the symmetric equilibrium becomes unstable to an antisymmetric perturbation when the freshwater forcing exceeds a threshold strength. At this bifurcation, the symmetric state makes a transition to an asymmetric state, rather than to a reversed symmetric circulation associated with deep-water formation in low latitudes. Furthermore, the destabilizing perturbation is of basin scale and is associated with a pole-to-pole overturning pattern.

A noteworthy result of the investigation due to Weijer and Dijkstra (2001) is that the symmetric steady state is more sensitive to antisymmetric perturbation than to symmetric ones. The main aim of the present study is to explore the physics underlying this behavior. For this purpose, we generalize the conceptual model of Nilsson and Walin (2001) for symmetric thermally dominated circulation, such that the stability to small antisymmetric perturbations can be analyzed. A key result of their investigation is that the features of the vertical mixing in the interior ocean are crucial for the stability of the circulation to symmetric perturbations: the symmetric flow is strongly stabilized if the vertical mixing increases with decreasing stability of the water column. Thus, a central question of the present study is whether the dynamics of antisymmetric perturbations are also sensitive to the nature of vertical mixing.

The presentation is structured as follows. Section 2 presents some results from a numerical simulation of the thermohaline circulation in a two-hemisphere basin. In Section 3, the model of Nilsson and Walin (2001) is recapitulated and its stability to small symmetric perturbations is briefly considered. In Section 4, a model describing antisymmetric perturbations on a symmetric circulation is developed and analyzed. The final section discusses the present results concerning the stability of symmetric thermohaline circulation in a broader context.

2. Salient results from a numerical simulation

2.1. Model description

We study thermohaline circulation in a two-hemisphere basin using the MIT ocean circulation model (Marshall et al., (1997a,b). The basin stretches from 60° south to 60° north, having a zonal width of 40° and a constant depth of 4400 m. The resolution is 2×2 deg^2, horizontally, with 26 vertical levels:

$$\tau_x = -\tau_{\max} \sin(2\pi y) \tan(\pi y/3), \tag{1}$$

where $y = \phi/\phi_N$ ranges from -1 (southern boundary) to $+1$ (northern boundary) and $\tau_{\max} = 0.2$ N m^{-2},

$$F_H = \lambda(T_S - T_R). \tag{2a}$$

Here, λ is the surface heat exchange coefficient, T_S the sea surface temperature and T_R is a reference temperature given by

$$T_R = \Delta T[\cos(\pi y) + 1]/2, \tag{2b}$$

where ΔT is the equator-to-pole temperature difference; λ is set to 45 W m^{-2} °C^{-1} and ΔT is set to 25 °C.

The salinity is forced by a freshwater flux at the surface

$$F_S = E_0 \cos(\pi y)/\cos(\pi y/3), \tag{3}$$

where E_0 gives the amplitude of the net evaporation per unit area. This idealized form captures the general pattern of net evaporation in low latitudes and net precipitation in high latitudes. Note that $E_0 = 1$ m yr^{-1} implies a poleward atmospheric freshwater transport of about 0.3 Sv at 30° latitude. A linear equation of state is used

$$\rho = \rho_0(1 - \alpha T + \beta S), \tag{4}$$

where ρ_0 is a constant reference density and $\beta = 8 \times 10^{-4}$ and $\alpha = 2 \times 10^{-4}$. The horizontal eddy viscosity and diffusivity are 5×10^3 and 10^3 m^2 s^{-1}, respectively, while the vertical eddy viscosity is 10^{-3} m^2 s^{-1}. The vertical diffusivity κ is uniform and is given the value 10^{-4} m^2 s^{-1}.

2.2. The transition from symmetric to asymmetric circulation

We are interested in the response of the symmetric circulation to a slow increase of the freshwater forcing. In the present two-hemisphere geometry, there is a single symmetric steady state associated with forward flow when the freshwater forcing is zero. As the forcing is increased, asymmetric steady states also become attainable. At some critical forcing strength, the symmetric circulation generally becomes unstable and undergoes a transition to an asymmetric steady state (e.g. Thual and McWilliams, 1992; Dijkstra and Molemaker, 1997; Klinger and Marotzke, 1999; Weijer and Dijkstra 2001). To study this transition, we have made a simulation in which the freshwater forcing increases linearly with time (starting from zero, the forcing reaches 0.5 m yr^{-1} after 10 000 yr). The rate of change in forcing is slow enough to allow the model to be in a symmetric quasi-steady state for several thousand model years. Figure 1 illustrates this quasi equilibrium at year 12 000. As shown in Fig. 2, a few hundred years later a transition to asymmetric circulation occurs. Over a few hundred years, the asymmetry of the flow increases rapidly until a new quasi-equilibrium is attained. Figure 3 shows the pronounced asymmetric circulation that has been reached in the model year 13 900. At this stage, the main reorganization of the hydrographic

[1]Note that unsteady boundary conditions, which may arise due to "weather noise" in coupled ocean–atmosphere models, generally are expected to reduce the stability of the "ocean-only" steady states considered here.

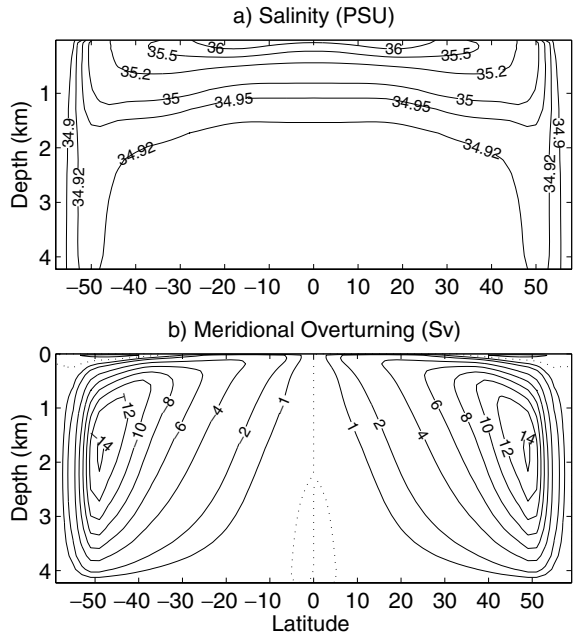

Fig 1. The symmetric circulation at the model year 12 000. The upper panel shows the zonally averaged salinity field and the lower panel shows the meridional overturning streamfunction; which is presented in units of Sverdrup (1 Sv = 10^6 m^3 s^{-1}).

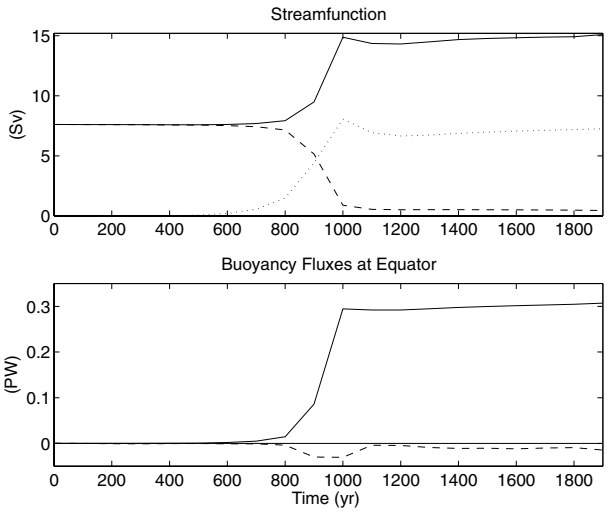

Fig 2. A time slice of the transition to asymmetric flow (starting from the model year 12 000) in an integration where the freshwater forcing increases linearly with time. Upper panel shows the maximum of the meridional streamfunction at 30° north (solid line), the equator (dotted line) and 30° south (dashed line). (Note the absolute value of the streamfunction is presented for 30° south.) The lower panel shows the northward thermal buoyancy flux (solid line) and the haline buoyancy flux (dashed line); note that both quantities are given as equivalent heat fluxes in units of petawatt.

fields has already occurred, but a slower diffusive adjustment is still in progress in the Southern Hemisphere deep ocean. It can be noted that the salinity range in the upper ocean is enhanced by the presence of low saline surface water in the stagnant Southern Hemisphere, where deep water production has ceased.

Consider next the perturbations that initialize the transition to asymmetry. To identify these anomalies, we take a pragmatic approach and view the equatorially antisymmetric parts of the haline and thermal field as small perturbations on a basic symmetric state. Similarly, the symmetric part of the meridional velocity is viewed as a perturbation on a basic antisymmetric field. This approach should be feasible in the very first phase of the transition. Figure 4 shows the perturbations in the zonally averaged density field and the meridional streamfunction. (It should be underlined that the perturbations have a nontrivial zonal structure; see Fig. 5.) In the initial growth phase depicted in Fig. 4, the density anomaly is concentrated towards high latitudes. The flow perturbation has a pole-to-pole structure with negligible upwelling/downwelling across the thermocline at low latitudes; the near equatorial overturning pattern in the deep ocean is encountered well below the thermocline. It should be recognized, however, that the total flow field is still nearly symmetric at this stage and is associated with net sinking at high latitudes. It is relevant to note that the structure of the fields that here we have assumed to be small perturbations are qualitatively similar to the structure of the perturbations that Weijer and Dijkstra (2001) found by solving the appropriate linear eigenvalue problem.

3. A conceptual model for symmetric circulation

Here, we summarize the model of Nilsson and Walin (2001) for symmetric thermohaline circulation. Their original one-hemisphere model is reformulated for a two-hemisphere basin with equatorially symmetric sea surface temperature (prescribed) and freshwater forcing. The predictive variables of the model are the circulation, the thermocline depth, and the equator-to-pole salinity contrast. The model is based on continuity of mass and salinity and employs the following dynamical assumptions.

(1) The flow is in hydrostatic and geostrophic balance, which yields the thermal wind relation

$$\frac{\partial v}{\partial z} = -\frac{g}{f\rho_0}\frac{\partial \rho}{\partial x}, \tag{5}$$

where v is the meridional velocity, z is the vertical coordinate, g is the acceleration of gravity, f is the Coriolis parameter, x is the zonal coordinate, ρ is the density and ρ_0 is the mean density.

(2) The stratification and the associated upwelling is governed by an advective–diffusive balance

$$w\frac{\partial \rho}{\partial z} = \frac{\partial}{\partial z}\left(\kappa\frac{\partial \rho}{\partial z}\right), \tag{6}$$

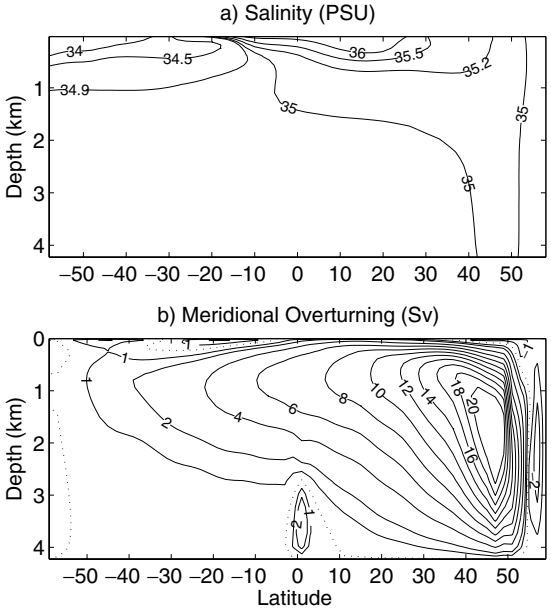

Fig 3. Asymmetric circulation at the model year 13 900. The upper panel shows the zonally averaged salinity field and the lower panel shows the meridional overturning streamfunction. It can be noted that the deep-water salinity has increased slightly and lies closer to mean salinity (35 PSU) than in the symmetric state.

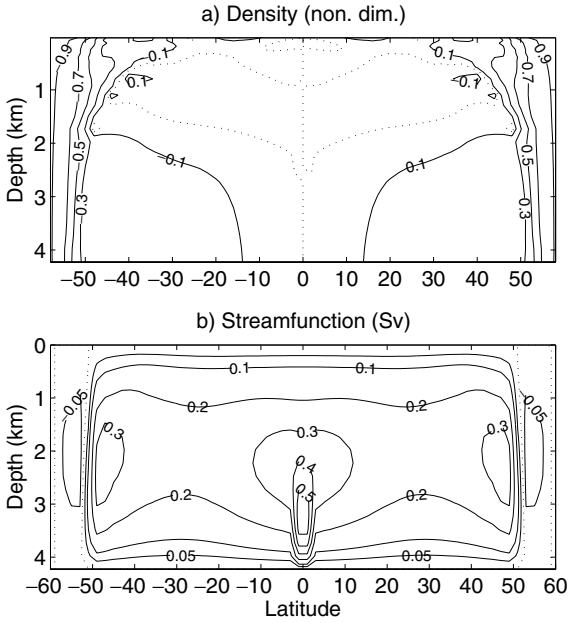

Fig 4. The perturbation on the basic state at year 12 700. The upper panel shows the zonal average of the antisymmetric component of the density field, which has been normalized by its maximum value (0.0023 kg m^{-3}). The lower panel shows the symmetric component of the streamfunction. This "antisymmetric" perturbation is associated with a positive density anomaly and enhanced sinking in the Northern Hemisphere. (For the sake of simplicity, the anomaly fields shown here will be referred to as an antisymmetric perturbation.)

where w is the vertical velocity and κ is the vertical diffusivity.

It should further be noted that the classical thermocline scaling, employed in this section to describe the overturning circulation, assumes that the thermocline depth is small compared with the depth of the ocean (e.g. Park and Bryan, 2000); this assumption will be relaxed in Section 4.2.

3.1. Conservation equations

We consider a two-hemisphere ocean model, as illustrated in Fig. 6. The model has an upper thermocline layer with depth H overlying an abyssal layer (these layers are distinguished by the subscripts e and p, respectively). For simplicity, the temperatures are prescribed: the thermocline temperature is T_e, while the temperature elsewhere is T_p. In consistency with the Boussinesq approximation, we demand continuity of volume

$$V = V_e + V_p,$$

where V is the volume of the entire basin. Furthermore, the area of the outcropping upper layer (A) is fixed, implying that $V_e = AH$. For the symmetric case considered here, the oceanic and atmospheric transports are equally strong in the two hemispheres. The poleward atmospheric freshwater transport is F, and the poleward transport and the upwelling, in each hemisphere, are denoted ψ_G and ψ_D, respectively. Conservation of volume and salinity are given by

$$\frac{A}{2}\frac{\mathrm{d}H}{\mathrm{d}t} = -\psi_G + \psi_D - F, \tag{7a}$$

$$\frac{1}{2}\frac{\mathrm{d}V_e S_e}{\mathrm{d}t} = -S_e\psi_G + S_p\psi_D, \tag{7b}$$

$$\frac{1}{2}\frac{\mathrm{d}V_p S_p}{\mathrm{d}t} = +S_e\psi_G - S_p\psi_D. \tag{7c}$$

An equation for the salinity difference, $\Delta S = S_e - S_p$, can be obtained from eqs. (7a)–(7c); straightforward manipulations yield

$$\frac{V_e}{2}\frac{\mathrm{d}\Delta S}{\mathrm{d}t} = -\Delta S[\psi_D + (V_e/V_p)\psi_G] + [S_e + (V_e/V_p)S_p]F.$$

By introducing the mean salinity, $S_0 = (S_eV_e + S_pV_p)/(V_e + V_p)$, the above formula can be rewritten as

$$\frac{V_e}{2}\frac{\mathrm{d}\Delta S}{\mathrm{d}t} = -\Delta S[\psi_D + (V_e/V_p)\psi_G + (V_e/V_p - 1)F] + S_0(1 + V_e/V_p)F.$$

We now make two geophysically motivated approximations.

(1) The atmospheric freshwater transport is taken to be small compared with the oceanic overturning, i.e.

$$F \ll \psi_G; F \ll \psi_D.$$

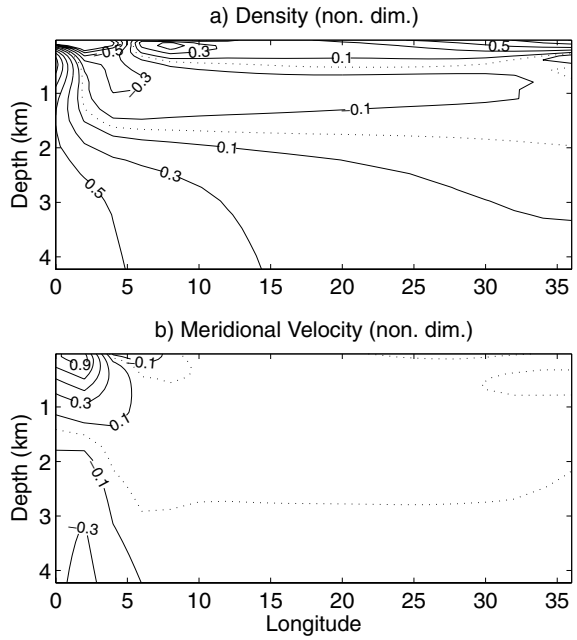

Fig 5. The zonal structure of the perturbations at 30° north (the model year 12 700). The upper panel shows the equatorially antisymmetric component of the density field and the lower panel shows the equatorially symmetric component of the meridional velocity. The fields have been normalized by their maximum values (0.0013 kg m^{-3} and 6.3×10^{-4} m s^{-1}, respectively) and the contour interval is 0.2 (the zero contour is dotted).

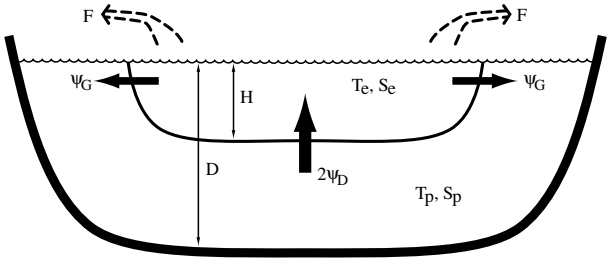

Fig 6. A two-layer model for equatorially symmetric circulation. Here, S and T denote salinity and temperature, respectively, ψ_G is the poleward flow, ψ_D is the upwelling and F is the poleward atmospheric moisture transport. Note that F is small compared to the oceanic transports and that the temperatures are assumed to be fixed. When ψ_G and ψ_D are parameterized, it is assumed that the basin depth D is large compared to the thermocline depth H.

This implies that $\Delta S \ll S_0$ when the system is in a steady state.

(2) The volume of the thermocline layer is taken to be small compared with that of the deep ocean, i.e.

$$V_e \ll V_p.$$

This approximation does not affect the steady-state solutions (provided that F is small) but simplifies the time-dependent equation for ΔS.

Making use of these approximations, we obtain the following simplified conservation equations:

$$\frac{A}{2}\frac{\mathrm{d}H}{\mathrm{d}t} = -\psi_G + \psi_D, \tag{8a}$$

$$\frac{AH}{2}\frac{\mathrm{d}\Delta S}{\mathrm{d}t} = -\Delta S\psi_D + S_0 F. \tag{8b}$$

The classical thermocline scaling (e.g. Welander, 1986) is used to derive representations of the flows ψ_G and ψ_D. A difference with respect to the standard treatment, which deals with a fixed vertical diffusivity, is that here we explore the consequences of a coupling between the diffusivity and the stratification. Straightforward scaling considerations of the thermal wind balance (eq. (5) governing ψ_G) and the advective diffusive balance (eq. (6) governing ψ_D) yield (see Nilsson and Walin, 2001; Nilsson et al. 2003, for details)

$$\psi_G = k_1 H^2 \Delta\rho, \tag{9a}$$

$$\psi_D = k_2 \Delta\rho^{-\zeta} H^{-\eta}. \tag{9b}$$

Here, we have introduced the two constants k_1 and k_2, and the density difference is given by

$$\Delta\rho = \Delta\rho_\mathrm{T} - \rho_0 \beta \Delta S, \tag{10}$$

where $\Delta\rho_\mathrm{T}$ is the density difference associated with the imposed thermal contrast. The parameters ζ and η can be adjusted to represent different relations between the vertical diffusivity and stratification; an issue that will be discussed below.

3.2. *Steady symmetric circulation*

Equations (8a)–(9b) provide a closed system that determines the symmetric steady-state solution for H, ΔS and the overturning circulation. From this solution it follows that ΔS increases with increasing freshwater forcing F, which reduces the density contrast $\Delta\rho$. However, this does not necessarily imply that the overturning strength also decreases with F, which has to do with the response of the pycnocline depth to the weaker density contrast. To demonstrate this, we use the steady-state version of eq. (8a) and define the overturning strength $\overline{\psi}$ according to

$$\overline{\psi} = \overline{\psi}_G = \overline{\psi}_D,$$

where we have introduced the convention of using the overbar to represent a stationary solution. By introducing $\overline{\psi}$ in eqs. (9a) and (9b) and eliminating H, we obtain a relation between the steady-state overturning and the density contrast:

$$\overline{\psi} = c\overline{\Delta\rho}^{\lambda}. \tag{11}$$

Here, we have introduced the parameter

$$\lambda = (\eta - 2\zeta)/(\eta + 2), \tag{12}$$

which depends on the relation between the vertical mixing and the stratification. (Note that the constant c may be expressed

in terms of k_1 and k_2 that appear in eqs. (9a) and (b.) Nilsson and Walin (2001) investigated the implications of three different mixing parameterizations.

(1) The commonly used assumption that the diffusivity is uniform and fixed, which leads to

$$\lambda = \frac{1}{3}; \quad (\eta = 1, \zeta = 0). \tag{13a}$$

(2) By assuming that $\kappa \propto N^{-1}$ (e.g. Gargett, 1984), where N is the buoyancy frequency, one obtains

$$\lambda = -\frac{1}{5}; \quad \left(\eta = \frac{1}{2}, \zeta = \frac{1}{2}\right). \tag{13b}$$

(3) If the rate of work performed against the buoyancy force by vertical mixing is constant, then $\kappa \sim \Delta\rho^{-1}$, which yields

$$\lambda = -\frac{1}{3}; \quad (\eta = 1, \zeta = 1). \tag{13c}$$

Thus in the present model, the overturning increases with increasing density contrast if the vertical diffusivity is taken to be fixed. However in the two latter cases, where the diffusivity declines with increasing stratification, a stronger equator-to-pole density difference will be associated with a weaker overturning. This rather remarkable impact of a coupling between the vertical mixing and the stratification has been demonstrated in simulations with ocean circulation models reported by Huang (1999) and Nilsson et al. (2003). The response of the thermocline depth (which according to eq. (9a) affects the overturning) is at the heart of this unexpected behavior. In a steady state, eqs. (9a) and (9b) lead to the relation

$$\overline{H} \propto \overline{\Delta\rho}^{(\lambda-1)/2}, \tag{14}$$

which shows that a weaker density difference is associated with a greater thermocline depth for all three mixing representations. However, the depth increase is larger in the two cases where the vertical mixing depends on the stratification, which results in a stronger overturning although the density difference has become smaller.

The steady-state properties of the model are governed by a single nondimensional parameter:

$$R = \frac{F\rho_0\beta S_0}{\overline{\psi}_{\mathrm{T}}\Delta\rho_{\mathrm{T}}}, \tag{15}$$

where $\overline{\psi}_{\mathrm{T}}$ is the overturning strength in the absence of freshwater forcing. This parameter can be interpreted as the ratio between the haline buoyancy flux and the thermal buoyancy flux for $F = 0$. As illustrated in Fig. (7), the mixing parameter λ affects the relation between the equilibrium salinity difference and the freshwater forcing: $\overline{\Delta S}$ increases more slowly with R when κ is assumed to depend on the stratification than when κ is assumed to be fixed.

Finally, it worth underlining that the above results concern the relation between the overturning dynamics and the nature of vertical mixing for flows that are symmetric with respect to the equator. The theoretical study by Saenko and Weaver (2003) indicates that asymmetric flows may behave differently. (They considered a conceptual model for asymmetric circulation in a basin with a circumpolar "Southern Ocean," where the combined effect of winds and eddy transports is assumed to drive upwelling of deep water. When the eddy transports are sufficiently strong in their model, the sinking in the Northern Hemisphere may increase with increasing equator-to-pole density difference regardless of whether the vertical diffusivity is taken to be constant or stratification dependent.)

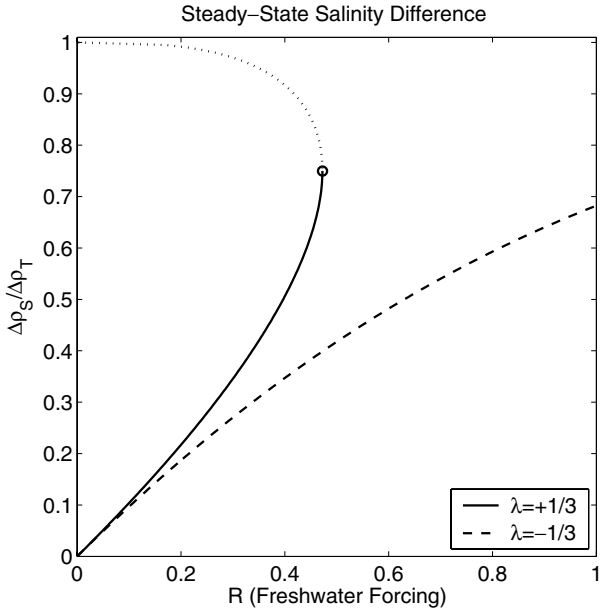

Fig 7. Steady-state salinity difference as a function of the nondimensional freshwater forcing R; see eq. (15). The salinity is nondimensionalized as $\rho_0\beta\Delta S/\Delta\rho_{\mathrm{T}}$. The solid line illustrates the case with constant vertical diffusivity, where the forward circulation becomes unstable to symmetric perturbations at a critical value of R (marked by a circle); the unstable branch of equilibria connecting this point is indicated by the dotted line. The case where the mixing energy is fixed (implying $\kappa \sim \Delta\rho^{-1}$), is illustrated by the dashed line. Note that this case is stable to symmetric perturbations for arbitrarily high values of R.

3.3. *Linear stability to symmetric perturbations*

Nilsson and Walin (2001) analyzed the linear stability of the steady-state solutions of eqs. (8)–(9b) to small equatorially symmetric perturbations of the thermocline depth and the salinity difference. Depending on the value of λ, they identified two distinct cases. First, the case $\lambda > 0$ where the steady state is stable provided that

$$\frac{\rho_0\beta\overline{\Delta S}}{\Delta\rho_{\mathrm{T}}} < \frac{1}{1+\lambda}. \tag{16}$$

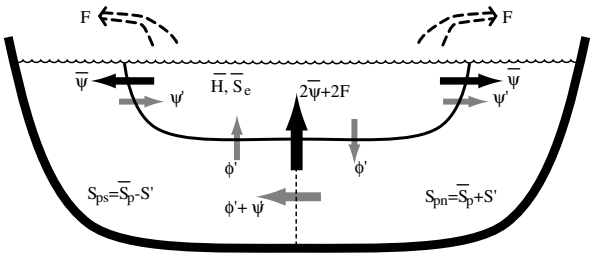

Fig 8. Illustration of an antisymmetric perturbation (denoted by primes) on the symmetric steady state (denoted by overbars). The anomalies of the deep-water salinity, the poleward flow, and the upwelling in the Northern Hemisphere are S', ψ' and $-\phi'$, respectively. Note that it is assumed that the perturbation does not affect the depth and the salinity of the upper layer. It is further assumed that, in both hemispheres, the net near-surface flows ($\overline{\psi} \pm \psi'$) are directed poleward and the net upwelling components ($\overline{\psi} + F \mp \phi\prime$) are positive; see eqs. (17c) and (17d).

Here the critical salinity difference—above which the flow is unstable to symmetric perturbations—depends on the mixing parameter λ. The standard two-box model of thermohaline circulation (where the box volumes are fixed and the flow is directly proportional to the density difference) essentially corresponds to the case $\lambda = 1$; which yields $\rho_0\beta\overline{\Delta S}/\Delta\rho_{\mathrm{T}} \leq \frac{1}{2}$. In the present two-layer model, however, the stabilizing effect due to the thermocline–depth adjustment pushes the critical salinity difference upwards; for a fixed vertical diffusivity (i.e. $\lambda = \frac{1}{3}$), eq. (16) yields $\rho_0\beta\overline{\Delta S}/\Delta\rho_{\mathrm{T}} \leq \frac{3}{4}$.

Second, the case where $\lambda < 0$. Here, the steady states of the model are always stable to symmetric perturbations. The reason is that a weaker density difference now is associated with a stronger circulation, which results in a negative feedback between salinity and flow anomalies.

4. Stability to antisymmetric perturbations

We proceed to analyze the stability of the symmetric circulation to small antisymmetric perturbations. The basic state is identical to the symmetric steady state described above. However, to treat antisymmetric perturbations we must allow the deep-ocean salinity to be different in the two hemispheres. The simplest way to describe this is to subdivide the reservoir V_p into one northern and one southern part, each having volume $V_p/2$; see Fig. 8. The salinity in these two reservoirs are

$$S_{p\mathrm{n}} = \overline{S}_p + S', \quad S_{p\mathrm{s}} = \overline{S}_p - S', \tag{17a}$$

where the subscripts n and s refer to the Northern and Southern hemispheres, respectively, and $\overline{S}_p$ is the steady-state salinity in the reservoir V_p.

Guided by our numerical results, we assume that the antisymmetric perturbations do not, as a first approximation, affect the depth and the salinity of the upper layer; see Fig. 4. Accordingly, we have in the perturbed state

$$S_e = \overline{S}_e, \quad H = \overline{H}, \quad V_{p\mathrm{n}} = V_{p\mathrm{s}} = \overline{V}_p/2. \tag{17b}$$

It should be noted that antisymmetric perturbations, in general, may affect the depth and the salinity of the upper layer in an asymmetric fashion. Thus, we have implicitly assumed that any asymmetric tendencies are curtailed by efficient communication within the upper layer, which keeps the salinity and the characteristic depth equal in the two hemispheres. If we make the opposite assumption, i.e. not allowing any communication across the equator, we will essentially recover a single-hemisphere case, for which the symmetric stability consideration in Section 3.3 applies. Accordingly, the assumption of perfect communication over the equator may be viewed as the most extreme antisymmetric case.

The perturbations on the flow components are defined as follows (see Fig. 8):

$$\psi_{G\mathrm{n}} = \overline{\psi} + \psi', \quad \psi_{G\mathrm{s}} = \overline{\psi} - \psi'. \tag{17c}$$

$$\psi_{D\mathrm{n}} = \overline{\psi} + F - \phi', \quad \psi_{D\mathrm{s}} = \overline{\psi} + F + \phi'. \tag{17d}$$

We emphasize that the flow perturbations are assumed to be so small that the net near-surface flows are directed poleward and the net upwelling is into the thermocline in both hemispheres. Note further that we have kept F in eq. (17d) despite the fact that it is small compared with $\overline{\psi}$, as we do not know a priori that it will be negligible in the stability analysis. We assume that the perturbations ψ' and ϕ' are coupled to the perturbation in deep-water salinity. A positive salinity perturbation in the Northern Hemisphere ($S' > 0$ implying a positive density anomaly) is expected to enhance the poleward flow in the Northern Hemisphere ($\psi' > 0$) while simultaneously decreasing the upwelling because of the increased vertical stability of the water column ($\phi' < 0$, applies if the mixing is stability dependent). Note that the volume of the upper layer is strictly conserved by these flow perturbations. From continuity, it follows that a cross-equatorial deep flow of strength $\psi' + \phi'$ is required as illustrated in Fig. 8.

Since the volumes $V_{p\mathrm{n}}$ and $V_{p\mathrm{s}}$ are constant, conservation of salinity for these two deep reservoirs can be expressed as

$$\frac{\overline{V}_p}{2}\frac{\mathrm{d}(\overline{S}_p + S')}{\mathrm{d}t} = \overline{S}_e(\overline{\psi} + \psi') - (\overline{S}_p + S')(\overline{\psi} + F - \phi') - (\overline{S}_p + S')(\psi' + \phi'), \tag{18a}$$

$$\frac{\overline{V}_p}{2}\frac{\mathrm{d}(\overline{S}_p - S')}{\mathrm{d}t} = \overline{S}_e(\overline{\psi} - \psi') - (\overline{S}_p - S')(\overline{\psi} + F + \phi') + (\overline{S}_p + S')(\psi' + \phi'), \tag{18b}$$

where eqs. (18a) and (18b) pertain to the northern and the southern deep ocean, respectively. We note that the last terms in these equations represent the cross-equatorial advection of salt in the deep ocean. The salinity conservation equations can be simplified by subtracting the stationary basic-state balance (i.e.

$\overline{S}_e\overline{\psi} - \overline{S}_p(\overline{\psi} + F) = 0$), which after some rearrangements leads to

$$\frac{\overline{V}_p}{2}\frac{\mathrm{d}S'}{\mathrm{d}t} = \overline{\Delta S}\psi' - S'(\overline{\psi} + F) - S'\psi',$$

$$-\frac{\overline{V}_p}{2}\frac{\mathrm{d}S'}{\mathrm{d}t} = -\overline{\Delta S}\psi' + S'(\overline{\psi} + F) + S'\psi' + 2S'\phi',$$

where as before $\overline{\Delta S} = \overline{S}_e - \overline{S}_p$. It should be noted that the term $2\,S'\,\phi'$ is not consistent with the assumed antisymmetry of the perturbations; it represents an exchange of salinity between the thermocline and the deep ocean in the Southern Hemisphere that has no counterpart in the Northern Hemisphere. Thus, the present model cannot treat antisymmetric perturbations of finite amplitude. In the limit of small perturbations, however, the quadratic terms can be neglected and the above equations describe a strictly antisymmetric perturbation:

$$\frac{\overline{V}_p}{2}\frac{\mathrm{d}S'}{\mathrm{d}t} = \overline{\Delta S}\psi' - S'\overline{\psi}. \tag{19}$$

Note that here we have used the assumption that $F \ll \overline{\psi}$ to simplify the last term. It is worth emphasizing that the upwelling perturbation ϕ' does not affect the antisymmetric salinity perturbation at leading order.

Two feedbacks can be identified in eq. (19). First, the negative feedback associated with the mean flow advection, i.e. the term $-S'\overline{\psi}$. (To be accurate, this attenuation of advected salinity anomalies is due to the vertical mixing in the upwelling branch.) Secondly, the advection of the mean salinity contrast by the flow perturbation, which is represented by $\overline{\Delta S}\psi'$. If the flow and salinity anomalies have the same sign, this term yields a positive feedback acting to destabilize the symmetric equilibrium. In this case, an inspection of eq. (19) reveals that the criteria for stability to antisymmetric salinity perturbation can be expressed as

$$\frac{\psi'}{\overline{\psi}} < \frac{S'}{\overline{\Delta S}}. \tag{20}$$

Thus, the symmetric circulation is stable if the relative perturbation in flow is smaller than relative perturbation in salinity. When this condition applies, small antisymmetric perturbations will decay exponentially with time. To put the general criteria (20) on a more quantitative basis, we will now explore the physics that couple ψ' and S'

4.1. *Walin's considerations*

Walin (1985) assumed that, in the mid to high latitudes, the antisymmetric flow anomaly ψ' locks on to the structure of the basic symmetric flow. Furthermore, he assumed that the flow anomaly obeyed the same dynamical relation as the symmetric poleward flow, i.e.

$$\overline{\psi} = k_1\overline{\Delta\rho H}^2, \quad \psi' = k_1\Delta\rho'\overline{H}^2, \tag{21}$$

where $\Delta\rho'$ is the density anomaly associated with the antisymmetric salinity perturbation (since the temperature field is assumed to be prescribed, the density perturbation is purely haline). This assumption implies that

$$\frac{\psi'}{\overline{\psi}} = \frac{\Delta\rho'}{\overline{\Delta\rho}}. \tag{22}$$

Furthermore, we have

$$\overline{\Delta\rho} = \Delta\rho_\mathrm{T} - \rho_0\beta\overline{\Delta S}, \quad \Delta\rho' = \rho_0\beta S'. \tag{23}$$

Since the salinity and flow perturbations have the same sign, the term $\overline{\Delta S}\psi'$ in eq. (19) acts to destabilize the symmetric equilibrium. To find the conditions under which the equilibrium is stable, we apply the above results to the stability condition (20), which yields

$$\frac{\rho_0\beta S'}{\Delta\rho_\mathrm{T} - \rho_0\beta\overline{\Delta S}} < \frac{S'}{\overline{\Delta S}}.$$

By simplifying this result, we find that the symmetric state is stable to antisymmetric perturbations if and only if

$$\frac{\rho_0\beta\overline{\Delta S}}{\Delta\rho_\mathrm{T}} < \frac{1}{2}. \tag{24}$$

Thus, the assumptions of Walin (1985) lead to a stability criteria given only in terms of the degree to which the salinity contrast has reduced the thermally imposed equator-to-pole density difference. It should be emphasized that this stability criteria is independent of the properties of vertical mixing, which proved to be crucial for the stability to symmetric perturbations. Furthermore, the antisymmetric instability arises at a salinity difference for which the flow still is stable to symmetric perturbations; see Section 3.3 and eq. (16). As shown in Fig. 7, however, the strength of the freshwater forcing that yields the critical salinity difference depends on the vertical mixing: a greater value of R is required to destabilize the flow with the stability-dependent mixing. Furthermore, it is relevant to note the criteria (24)—derived here for a two-layer model—is the same as the stability criteria for Stommel's classic two-box model under mixed boundary conditions (e.g. Marotzke 1996). The reason is that, despite their different physical settings, Stommel's as well as our analyses assume the relation (22).

4.2. *Flow amplification by deep ocean density gradients*

In the above analysis, it was tacitly assumed that the flow perturbation is generated by horizontal density gradients within the thermocline. Thus, the deep ocean was viewed as dynamically passive. However, the assumed structure of the antisymmetric density (salinity) perturbation has in fact an interhemispheric gradient extending over the whole depth of the basin. This suggests that there may also be substantial deep zonal density variations, which must be associated with a meridional deep flow. The view that the deep ocean plays a dynamically active role is further corroborated by the numerical simulation, which yielded an antisymmetric density perturbation that has meridional as well

as zonal gradients below the thermocline (see Figs. 4 and 5). As will be shown, such deep density gradients may well enhance the thermocline flow perturbation ψ', thereby making the symmetric flow more unstable. We now try to estimate an upper bound for the strengthening of ψ' due to density gradients in the deep ocean. For this purpose, we relax the requirement that the thermocline depth ($\overline{H}$) should be much smaller than the basin depth (say D), which was invoked in Section 3. In fact, the classical thermocline scaling that was employed to describe the symmetric overturning concerns the limiting case where $\overline{H}/D$ approaches zero (e.g. Park and Bryan, 2000).

Let us assume that the salinity perturbation, in say the northern part of the basin, is distributed so that the salinity difference between the western and the eastern boundary is S' all the way from the surface to the bottom. The positive density anomaly in the western part of the basin will, in accordance with the thermal-wind relation, be associated with a meridional flow that increases towards the sea surface. As a consequence of mass conservation, there should thus be a net northward flow in the upper half of the ocean and a compensating southward flow underneath. Specifically, we assume that the perturbation in the east–west density difference is vertically uniform and has the strength $\Delta\rho'$. By integrating the thermal-wind relation (5) vertically and meridionally and demanding mass continuity, we find the associated flow perturbation has the following vertical distribution:

$$\int v' \mathrm{d}x = \frac{g\Delta\rho'}{\rho_0 f}(z + D/2). \tag{25}$$

Here, the integral spans the whole basin, and v' is the meridional velocity perturbation and D is the basin depth. It can be noted that, due to mass conservation, the flow perturbation reverses sign at the mid depth $z = -D/2$.

We anticipate that this deep flow structure will augment the northward flow of thermocline water (ψ_{Gn}) by strengthening the perturbation ψ'. It should be recognized that it is not the net poleward volume transport by itself that matters for the stability of the symmetric flow. Rather, it is the anomalous salinity transport that affects the stability; see eq. (19). Since $\overline{\Delta S}$ is taken to be zero below the thermocline in the present model (in agreement with the numerical results shown Fig. 3), it is the northward perturbation in transport between the surface and the thermocline that drives the anomalous salinity flux. This transport is obtained by integrating eq. (25) over the upper layer (from $-\overline{H}$ to 0), which yields

$$\psi' = \frac{g\Delta\rho' D\overline{H}}{2\rho_0 f}(1 - \overline{H}/D). \tag{26}$$

In order to use this result in our stability condition (24), we need an estimate of $\overline{\psi}$ that accounts for the effects of a finite $\overline{H}/D$ ratio. For this purpose, we assume that the east–west density difference of the basic state is constant in the thermocline, where it equals $\overline{\Delta\rho}$, and is zero in the deep ocean. By straightforward application of the thermal-wind balance and mass conservation, we find that the zonal integral of the meridional velocity is distributed vertically as

$$\int \overline{v}\mathrm{d}x = \frac{g\overline{\Delta\rho}}{\rho_0 f}\left(z + \overline{H} - \frac{\overline{H}^2}{2D}\right), \quad 0 \geq z \geq -\overline{H};$$

$$\int \overline{v}\mathrm{d}x = -\frac{g\overline{\Delta\rho}\overline{H}^2}{\rho_0 f 2D}, \quad -\overline{H} \geq z \geq -D.$$

By integrating the above result over the thermocline layer, we arrive at

$$\overline{\psi} = \frac{g\overline{\Delta\rho}\overline{H}^2}{2\rho_0 f}(1 - \overline{H}/D). \tag{27}$$

It is relevant to note that this formula reduces to the estimate given by eq. (9a) in the limit $\overline{H}/D \ll 1$.

We proceed to analyze the stability of symmetric flow. To begin with, eqs. (26) and (27) lead to the relation

$$\frac{\psi'}{\overline{\psi}} = (D/\overline{H})\frac{\Delta\rho'}{\overline{\Delta\rho}}. \tag{28}$$

In comparison with eq. (22), the assumption of a deep east–west density difference leads accordingly to a considerable amplification of the antisymmetric flow perturbation. To arrive at a rough estimate of this amplification, we take a thermocline depth of 1 km and a basin depth of 4 km, which suggests that $D/\overline{H} \sim 4$. Making use of the stability condition (20) in combination with eqs. (23) and (28), we find that the symmetric state is now stable to antisymmetric perturbations provided that

$$\frac{\rho_0\beta\overline{\Delta S}}{\Delta\rho_T} < \frac{\overline{H}}{D + \overline{H}}. \tag{29}$$

Since the basin depth is an extreme upper bound on the thermocline depth, the right-hand side of eq. (29) is always less than one half. A comparison with the stability criteria given by eq. (24) shows that an amplification of the flow perturbation due to deep-ocean density gradients lowers the stability threshold. Furthermore, this destabilizing effect is more pronounced if the thermocline depth is small compared with the ocean depth.

It should be emphasized that the stability criteria (29) was derived without assuming that the ratio between thermocline depth and the basin depth is small; an assumption that was invoked when the symmetric states were considered in Section 3. However, the criteria (29) is implicit as the thermocline depth is some function of the salinity contrast. To obtain an approximate but explicit stability criteria we employ the thermocline–depth relation (14), which is strictly valid only if $\overline{H}/D \ll 1$. The result is summarized in Fig. 9, showing the critical salinity difference as a function of the nondimensional basin depth D/H_T, where H_T is the thermocline depth that the model yields when $F = 0$. We deem that a reasonable upper limit of the thermocline depth is $\overline{H} = D/2$, which from eq. (29) yields $\frac{1}{3}$ as an upper bound of the critical salinity difference. Accordingly, the graphs in Fig. 9 presumably overestimate the critical salinity difference when D/H_T is less than about 3. Keeping this caveat in mind, it

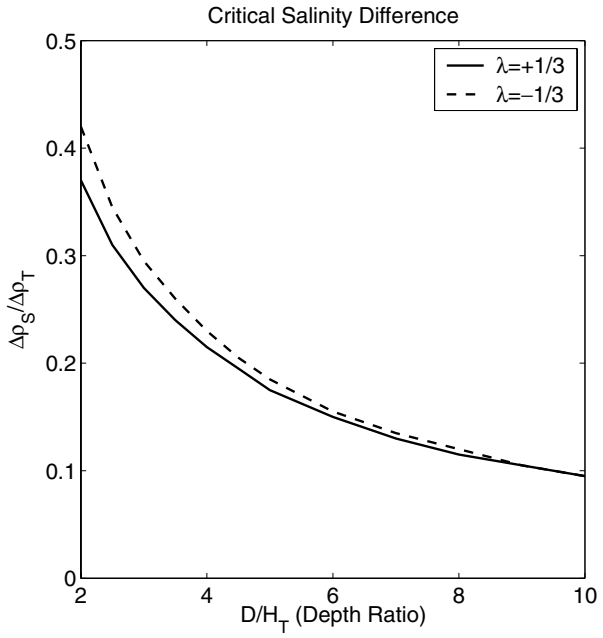

Fig 9. The critical salinity difference, calculated from eq. (29), as a function of the basin depth. For a greater salinity difference, the symmetric circulation is unstable to antisymmetric perturbations. The salinity difference and the basin depth are nondimensionalized as $\rho_0\beta\Delta S/\Delta\rho_T$ and D/H_T, respectively (where H_T is the thermocline depth when $R = 0$). The solid and dashed lines indicate the cases with constant vertical diffusivity and constant mixing energy, respectively. Note that the critical salinity difference predicted from eq. (29) is always less than $\frac{1}{2}$; which is the prediction from eq. (24).

is nevertheless clear that the symmetric flow becomes unstable for a weaker salinity difference when the basin is deep and the reference thermocline H_T is shallow. It can be noted that the stability-dependent mixing moves the critical salinity difference slightly upwards. But to the lowest order of approximation, the stability condition is independent of the features of the vertical mixing. For larger values of D/H_T, the stability criteria is well approximated by

$$\frac{\rho_0\beta\overline{\Delta S}}{\Delta\rho_T} < \frac{H_T}{D}. \tag{30}$$

Note that the properties of vertical mixing also enter implicitly in this relation since the reference thermocline depth obeys

$$H_T \propto \Delta\rho_T{}^{(\lambda-1)/2}.$$

Accordingly, a greater thermal density contrast $\Delta\rho_T$ reduces the value of $\rho_0\beta\overline{\Delta S}/\Delta\rho_T$ at which the symmetric circulation becomes unstable. Note that this applies for the constant as well as the stability-dependent diffusivity representations. Finally, we underline that although the critical salinity predicted from eq. (29) depends only weakly on the properties of the vertical mixing; the relation between the steady-state salinity difference and the freshwater forcing is sensitive to the assumed features of the mixing as illustrated in Fig. 7.

5. Discussion

The present conceptual stability analysis of symmetric thermohaline circulation shows that the system is more sensitive to antisymmetric than to symmetric perturbations; the antisymmetric instability arises for a smaller equator-to-pole salinity difference than does the symmetric one. An underlying reason is that the symmetric perturbations are associated with changes of the thermocline depth, which provide a forceful negative feedback. The pole-to-pole overturning pattern of the antisymmetric perturbations essentially short-circuits the stabilizing thermocline feedback. Furthermore, the antisymmetric flow perturbations can be augmented by interhemispheric density anomalies in the deep ocean, which then serves as a powerful positive feedback. Another noteworthy result is that while the symmetric perturbations are sensitive to the features of vertical mixing, the antisymmetric ones are not. These results may serve to explain why the breakdown of symmetric thermally dominated circulation in numerical simulations is generally associated with the emergence of an asymmetric circulation rather than a reversed symmetric circulation (Thuals and McWilliams, 1992 ; Dijkstra and Molemaker 1997; Klinger and Marotzke, 1999; Weijer and Dijkstra, 2001).

The main original result is the stability criteria for antisymmetric perturbations given by eq. (29), which is a generalization of the result (eq. (24)) presented by Walin (1985). These two criteria may be viewed as limiting cases. If we assume that interhemispheric density gradients in the deep ocean do not affect the antisymmetric flow perturbations at all, we obtain the criteria (24). The extreme opposite case results if we assume that the perturbation is associated with an east–west density difference that penetrates undiminished to the bottom of the ocean. This leads to the criteria (29), which depends on the basin depth and always yields a lower threshold value than eq. (24). Accordingly, we anticipate that the antisymmetric instability arises for a salinity difference that lies between the values given by eqs. (29) and (24). We underline that this estimated range serves as a lower bound on the critical salinity difference, as we have assumed that the temperature field does not change. Restoring boundary conditions on the sea-surface temperature generally stabilizes the flow, thereby raising the critical salinity difference. The effects of wind-driven circulation should also serve to stabilize the thermohaline flow.

The results from the numerical simulation are in broad agreement with the theoretical results. When the asymmetry starts to develop (near the model year 12 000) the salinity field has removed about 30% of the equator-to-pole density difference associated with the temperature field, i.e. $\Delta\rho_S/\Delta\rho_T \approx 0.3$. Already the fact that the instability arises when $\Delta\rho_S/\Delta\rho_T < \frac{1}{2}$ suggests that deep density gradients enhance the antisymmetric flow perturbation; not least since the restoring thermal boundary conditions and the wind forcing should act to stabilize the simulated symmetric circulation. This view is further corroborated by an

inspection of Fig. 5, which shows that the antisymmetric density anomaly that arises in the numerical model has zonal gradients that extend over the whole basin depth. However, it is beyond the scope of the present work to undertake a qualitative investigation of the coupling between the deep-ocean interhemispheric density gradient and the antisymmetric flow perturbation. As a concluding remark on the numerical results, it should be emphasized that we have employed a fixed vertical diffusivity in the simulation reported here. Thus, it would be interesting to investigate numerically whether the antisymmetric perturbations are essentially insensitive to the features of vertical mixing, as the present conceptual model suggests.

We emphasize that the present idealized study concerns the stability of a symmetric thermohaline circulation in a two-hemisphere basin. In the World Ocean, on the other hand, there are several ocean basins and the thermohaline circulation is presently in an equatorially asymmetric state. However, there is a qualitative prediction of eq. (29) that may be of palaeoceanographic interest, namely the stability of a symmetric thermohaline circulation depends on the ratio between the thermocline and the basin depth. The mean depth of the ocean has presumably varied only marginally over the last 100 Myr. The thermocline depth, however, may have changed considerably since it depends on the equator-to-pole temperature difference. For instance, during the Paleogene and the Eocene some 40–50 Ma, the equator-to-pole temperature difference in the ocean may have been only 15 °C, or even weaker (Huber and Wing 2000). This weaker temperature contrast should have been associated with a deeper thermocline; a state of affairs that according to eq. (29) should serve to stabilize the symmetric state. Although the degree of asymmetry of the circulation in the ancient oceans is not known in any detail, the present considerations suggest that climates with weak equator-to-pole temperature differences should favor the symmetric mode of thermohaline circulation.

6. Acknowledgments

This work was supported by the Swedish Science Research Council and by MISTRA through the SWECLIM program. We wish to thank two reviewers for their insightful comments and suggestions. We further thank the Knut and Alice Wallenberg Foundation for funding the Linux Cluster “Otto” and the staff at the National Center for Super Computing in Linköping for their assistance.

References

Bryan, F. 1986. High-latitude salinity effects and interhemispheric thermohaline circulations. *Nature* **323**, 301–323.

Dijkstra, H. A. and Molemaker, M. J. 1997. Symmetry breaking and overturning oscillations in thermohaline-driven flows. *J. Fluid Mech.*, **331**, 169–198.

Dijkstra, H. A. and Neelin, J. D. 2000. Imperfections of the thermohaline circulation: latitudinal asymmetry and preferred northern sinking. *J. Climate* **13**, 366–382.

Gargett, A. E. 1984. Vertical eddy diffusivity in the ocean interior. *J. Mar. Res.* **42**, 359–393.

Huang, R. X. 1999. Mixing and energetics of the oceanic thermohaline circulation. *J. Phys. Oceanogr.* **29**, 727–746.

Huber, B. T. and Wing, K. G. M. S. L. 2000. *Warm Climates in Earth History* 1st edn. Cambridge University Press, Cambridge, 462pp.

Klinger, B. A. and Marotzke, J. 1999. Behavior of double-hemisphere thermohaline flows in a single basin. *J. Phys. Oceanogr.* **29**, 382–399.

Marotzke, J., 1996. Analysis of thermohaline feedbacks. In: *Decadal Climate Variability; Dynamics and Predicatbility*, eds.D. L. T. Anderson and J. Willebrand, Vol. I, Springer-Verlag, Berlin, 334–378.

Marotzke, J., Welander, P. and Willebrand, J. 1988. Instability and multiple steady states in a merdional-plane model of the thermohaline circulations. *Tellus* **40A**, 162–172.

Marshall, J., Adcroft, A., Hill, C., Perleman, L. and Heisey, C., 1997a. A finite-volume, incompressible Navier Stokes model for studies of the ocean on parallel computers. *J. Geophys. Res.* **103, C3**, 5753–5766.

Marshall, J., Hill, C., Perleman, L. and Adcroft, A. 1997b. Hydrostatic, quasi-hydrostatic, and non-hydrostatic ocean modeling. *J. Geophys. Res.* **103, C3**, 5733–5752.

Nilsson, J. and Walin, G. 2001. Freshwater forcing as a booster of thermohaline circulation. *Tellus* **53A**, 628–640.

Nilsson, J., Broström G. and Walin G., 2003. The thermohaline circulation and vertical mixing: does weaker density stratification give stronger overturning? *J. Phys. Oceanogr.* **33**, 2781–2795.

Park, Y.-G. and Bryan, K. 2000. Comparison of thermally driven circulation from a depth-coordinate model and an isopycnal model. Part I: scaling-law sensitivity to vertical diffusivity. *J. Phys. Oceanogr.* **30**, 590–605.

Pickard, G. L. and Emery, W. J. 1982. *Descriptive Physical Oceanography* 4th edn. Pergamon Press, Oxford, 249 pp.

Rooth, C. 1982. Hydrology and ocean circulation. *Prog. Oceanogr.* **11**, 131–149.

Saenko, O. A. and Weaver, A. J. 2003. The effect of Southern Ocean upwelling on the global overturning circulation. *Tellus* **55A**, 106–111.

Scott, J. R., Marotzke, J. and Stone, P. H. 1999. Interhemispheric thermohaline circulation in coupled box model. *J. Phys. Oceanogr.* **29**, 351–365.

Thual, O. and McWilliams, J. C. 1992. The catastrophe structure of thermohaline convection in a two-dimensional fluid model and comparison with low-order box models. *Geophys. Astrophys. Fluid Dyn.* **64**, 67–95.

Walin, G. 1985. The thermohaline circulation and the control of ice ages. *Palaeogeogr., Palaeoclimatol., Palaeoecol.* **50**, 323–332.

Weijer, W. and Dijkstra, H. A. 2001. A bifurcation study of the three-dimensional thermohaline circulation: the double hemispheric case. *J. Mar. Res.* **59**, 599–631.

Welander, P. 1986. Thermohaline effects in the ocean circulation and related simple models. In: *Large-scale Transport Processes in the Oceans and Atmosphrere*, (eds. J. Willebrand and D. L. T. Anderson). Reidel, Dordrecht, 163–200.